www.sciencemag.org/cgi/content/full/333/6040/345/DC1

Supporting Online Material for

Electrical Spiking in *Escherichia coli* Probed with a Fluorescent Voltage-Indicating Protein

Joel M. Kralj, Daniel R. Hochbaum, Adam D. Douglass, Adam E. Cohen*

*To whom correspondence should be addressed. E-mail: cohen@chemistry.harvard.edu

Published 15 July 2011, *Science* **333**, 345 (2011)
DOI: 10.1126/science.1204763

This PDF file includes:

Materials and Methods
SOM Text
Figs. S1 to S11
Tables S1 to S6
Movie captions S1 to S7
References

Other Supporting Online Material for this manuscript includes the following:
(available at www.sciencemag.org/cgi/content/full/333/6040/345/DC1)

Movies S1 to S7

Materials and Methods

Construction of PROPS and pHluorin

Green absorbing proteorhodopsin strain EBAC31A08 *(3)* (GenBank AF279106) was used in a pBAD TOPO plasmid for arabinose induction or in a pACYC184 plasmid for IPTG induction. The D97N mutant was made using the QuikChange II kit (Stratagene) with the primers 5'-CGT CCC CCG GTA CAT CAA CTG GAT TCT CAC AAC-3' and the reverse complement 5'-GTT GTG AGA ATC CAG TTG ATG TAC CGG GGG ACG-3' (Integrated DNA Technologies). Mutants were checked by sequencing (Genewiz).

A plasmid containing super-ecliptic pHluorin*(9)* (GenBank AY533296) was a kind gift of Gero Meissenbock. The gene was cloned into a pCDF-Duet vector (Novagen) using forward BamH1 and reverse NotI restriction sites. Proper insertion of the gene was checked by sequencing. For dual expression of PROPS and pHluorin, the pACYC184 plasmid with GPR D97N and the pCDF-Duet plasmid were serially transduced into *E. coli* strain BL21.

A fusion of PROPS and the fluorescent GFP homolog Venus *(18)* was created by PCR sewing the fluorescent protein into the pBAD vector. The proper insertion of Venus was checked by sequencing. The fusion construct was transfected into strain BW25113.

E. coli growth

PROPS was expressed in five strains of *E. coli* (Table S1). Cells were grown to early-log phase (OD600 = 0.3 – 0.4) in 50 mL of LB medium in a shaking incubator at 33 ^{o}C. Inducer was added along with all-*trans* retinal (5 μM from a 20 mM stock in ethanol) and further growth was conducted in the dark. Cells were harvested after 3.5 hours and washed with 30 mL of minimal medium (1x M9 salts, 0.4% glucose, pH 7). Cells were resuspended in 5 mL minimal medium and used immediately or stored at 4 ^{o}C for up to two weeks. All experiments were performed at room temperature, except for monitoring growth on an agarose pad which was performed at 35 ^{o}C.

Protein purification

PROPS was expressed in *E. coli* and purified, following Ref. *(19)*. Briefly, cells (strain UT5600, pBAD TOPO plasmid) were grown in 1 L of LB with 100 μg/mL ampicillin, to an O.D 600 of 0.4 at 37 °C. All-*trans* retinal (5 μM) and inducer (arabinose 0.02%) were added and cells were grown for a further 3 hours. Cells were harvested by centrifugation and resuspended in 50 mM Tris, 2 mM $MgCl_2$ at pH 7 and lysed with a tip sonicator for 5 minutes. The lysate was centrifuged and the pellet was resuspended in PBS supplemented with 1.5% octyl glucoside (OG). The mixture was homogenized with a glass/teflon Potter Elvehjem homogenizer and centrifuged again. The sample was passed through a Ni-agarose column (Qiagen) for purification, and bound protein was eluted with 400 mM imidazole. The imidazole was removed by dialysis against a solution of 1% OG in PBS.

Super-ecliptic pHluorin was expressed with a HIS tag and purified following standard procedures.

Purification of inner membrane

Inner membranes were purified following a modification of the protocol of Ref. *(20)*. *E. coli* strain BW25113 was grown as in table S2. 5 mL of cultured cells were harvested by

centrifugation and resuspended in a chilled solution of 20% (weight:weight) sucrose in buffer of 500 mM potassium phosphate, 5 mM magnesium sulfate, and 1 mM phenylmethylsulfonyl fluoride (PMSF), pH 7.5. The suspension was passed through a French press at 8000 psi. The resulting solution was centrifuged for 10 min. at 3000 g. Cell membranes remained in the supernatant and were collected. Next, 20% sucrose in buffer described above (without PMSF), was added to bring the solution to 7 mL. A polyallomer centrifuge tube (Beckman Coulter) was filled sequentially with 1 mL 65% (w:w) sucrose in buffer, 4 mL 40% (w:w) sucrose in buffer, and the 7 mL of 20% sucrose solution with cell membranes. Tubes were spun in an ultracentrifuge with a SW41 rotor at 39,000 RPM for 16 hours at 4 ºC. Inner membranes segregated to the interface between the 20% and 40% sucrose solutions, while the outer membrane collected between the 40% and 65% sucrose solutions. We observed that the inner membranes remained pink while the outer membranes did not, implying that PROPS localized to the inner membrane.

Spectroscopic measurements

Absorption spectra of purified GPR WT and PROPS were recorded on a QE65000 spectrometer (Ocean Optics) equipped with a white-light LED illuminator. Fluorescence excitation and emission spectra were recorded on a Cary Eclipse fluorimeter (Varian) on purified PROPS solubilized in 1% octyl glucoside.

The quantum yield (QY) was calculated by comparison of the absorption and emission spectra of PROPS to corresponding spectra of Alexa 647 (112 pM in PBS, Molecular Probes). The QY of PROPS was calculated by

$$QY_{PROPS} = \frac{em_{PROPS}}{em_{AF647}} \frac{abs_{AF647}}{abs_{PROPS}} QY_{AF647}$$

where *abs* is the absorbance of the sample at 633 nm and *em* is the integrated fluorescence emission over the range 650 nm – 750 nm for both species. The quantum yield of Alexa 647 is 0.33. The quantum yield obtained by this procedure was 1.0×10^{-3}.

To determine pH-dependent fluorescence, the pH of the PROPS solution was changed with NaOH and measured using a microtip pH meter.

Fluorescence imaging

Cells were imaged in a home-built inverted fluorescence microscope equipped with a dual-view emission pathway. Illumination was provided either in *tran*s or *epi*. The light sources used in the experiments are given in Table S3. The microscope was equipped with a high numerical aperture (N.A. 1.45) 60 X oil-immersion objective (Olympus), enabling through-the-objective total internal reflection fluorescence (TIRF) imaging. The cameras were frame-transfer EMCCDs (Andor iXon^{+}) with either 512 x 512 pixels (for imaging a large field of view) or 128 x 128 pixels (for high-speed imaging).

For imaging of PROPS fluorescence alone, the 633 nm HeNe was used for excitation, and a Cy5 filter set (λ_{exc} = 633 nm, λ_{em} = 660-760 nm) was used to separate emission from excitation. Blinking was typically observed with an electron-multiplying gain of 300 and an exposure of 100 ms.

For simultaneous imaging of a fluorophore and PROPS, light from either the 532 nm laser, the 488 nm laser, or the supercontinuum source was combined with the 633 nm excitation using a 590 DCXR dichroic mirror (Chroma). A multi-band dichroic (Semrock Di01-R405/488/561/635) was used in the microscope to separate emission from excitation.

Alternatively, in some cases the combined laser beams were brought in the *trans* configuration, in which case no dichroic mirror was used.

A two-color imaging system was constructed to image two fluorophores simultaneously on one camera. A variable slit (ThorLabs) was placed in the image plane to select a rectangular region of the image with an aspect ratio of approximately 2:1. A dichroic mirror (640 DCXR Chroma) separated the fluorescence into a long-wavelength path and a short-wavelength path. A 710/100 emission filter (Chroma) selected the emission from PROPS in the long-wavelength path, and a 580/60 filter selected the emission from pHluorin or TMRM in the short wavelength path. The beams were recombined on a second 640 DCXR dichroic mirror and imaged onto the EMCCD camera. For single color imaging, the variable slit was removed and one emission path blocked.

Through-the-objective TIRF imaging was used to observe TMRM because out of focus dye would otherwise overwhelm the signal from dye taken up by the *E. coli*.

Photobleaching of PROPS and Venus

To compare the photostability of PROPS and Venus, we recorded photobleaching traces of both, in a PROPS-Venus fusion. By measuring photobleaching on the fusion protein, and for both fluorochromes in the same sample, we ensured that an equal number of molecules of PROPS and Venus contributed to their respective signals. This 1:1 stoichiometry facilitated calculation of the relative number of photons emitted prior to photobleaching.

E. coli expressing the PROPS-Venus fusion were treated with CCCP to set $V_m = 0$ and $pH_i = pH_o$. Cells were adhered to a glass coverslip pre-treated with poly-L-lysine and imaged in minimal medium at pH 7.5.

Photobleaching of PROPS and Venus were measured sequentially on the same sample under wide-field laser illumination. PROPS was excited at λ_{exc} = 633 nm, with emission collected through a 710/100 nm bandpass filter. Venus was excited at λ_{exc} = 488 nm, with emission collected through a 550/50 nm bandpass filter. The laser powers were adjusted so that the initial fluorescence intensities were approximately equal for PROPS and Venus. For both fluorochromes, a background signal from a cell-free region of the sample was subtracted from the raw intensity. Intensities were then corrected for the wavelength-dependent quantum yield of the EMCCD and the overlap between the emission spectrum of the fluorochrome and the transmission spectrum of the corresponding band pass filter. The photobleaching decays were fit to a single exponential, and the relative areas under the fits for the two fluorochromes determined the relative number of total photons prior to photobleaching.

Estimate of the number of molecules of PROPS per cell

We determined the average number of molecules of PROPS per cell by measuring the amount of retinal required to saturate the binding. Free and bound retinal were spectroscopically distinguishable by their visible absorption maxima, at 380 and 555 nm, respectively. At low retinal concentrations, most added retinal was taken up by PROPS. Once the PROPS was saturated, additional retinal remained free.

Addition of retinal drove the reaction:

$$\text{Ret} + \text{Ops} \rightleftharpoons \text{PROPS}$$

with equilibrium constant K_{eq}. In this scheme Ops is the microbial opsin without retinal, and PROPS is the assembled complex. The spectroscopically measureable concentrations were [Ret]

and [PROPS]. The amount of retinal added was $[R^{(0)}]$ = [Ret] + [PROPS]. Our goal was to determine $[P^{(0)}]$ = [Ops] + [PROPS].

A 50 mL culture of *E. coli* strain BW25113 was grown to OD 0.4 and induced with 0.0005% arabinose, following the usual procedure for preparing cells for imaging. After 3.5 hours the cells were split into 20 aliquots of 1 mL, and to each was added a known quantity of retinal. The retinal concentrations varied from zero to 45 μM. The cells were incubated with retinal overnight at 4 ºC.

Visible absorption measurements were taken on whole cells using a QE65000 spectrometer (Ocean optics). Cells expressing protein but without retinal were used as a reference to correct for scattering. A white LED (LuxeonV) provided illumination. Analysis was performed in Matlab.

Absorption spectra had two peaks, corresponding to free retinal (λ_{max} = 380 nm) and retinal bound to PROPS (λ_{max} = 555 nm). Singular Value Decomposition (SVD) *(21)* was applied to identify the spectral components that co-varied with retinal concentration. The two principal spectra returned by SVD appeared to be linear combinations of the spectra of free and bound retinal, so we generated two new basis functions by taking linear combinations that matched spectra of free and bound retinal. A projection of the measured spectrum onto these reference spectra was then performed at each retinal concentration to determine the concentrations of the free and bound retinal.

The concentrations of the measureable species are given by:

$$[\text{PROPS}] = \frac{1 + K_{eq}\left(\left[P^{(0)}\right] + \left[R^{(0)}\right]\right) - \sqrt{-4\left[P^{(0)}\right]\left[R^{(0)}\right]K_{eq}^2 + \left(1 + K_{eq}\left(\left[P^{(0)}\right] + \left[R^{(0)}\right]\right)\right)^2}}{2K_{eq}}$$

and

$$[\text{Ret}] = \frac{-1 + K_{eq}\left(\left[R^{(0)}\right] - \left[P^{(0)}\right]\right) + \sqrt{-4\left[P^{(0)}\right]\left[R^{(0)}\right]K_{eq}^2 + \left(1 + K_{eq}\left(\left[P^{(0)}\right] + \left[R^{(0)}\right]\right)\right)^2}}{2K_{eq}}.$$

The ratio [Ret]/[PROPS] was fit as a function of $[R^{(0)}]$ yielding values K_{eq} = 0.5 μM^{-1} and $[P^{(0)}]$ = 5.5 μM (Figure below).

A cell count on a hemocytometer yielded a density of 1.2×10^{11} cells/mL, whereupon we calculated 28,000 molecules of PROPS per cell.

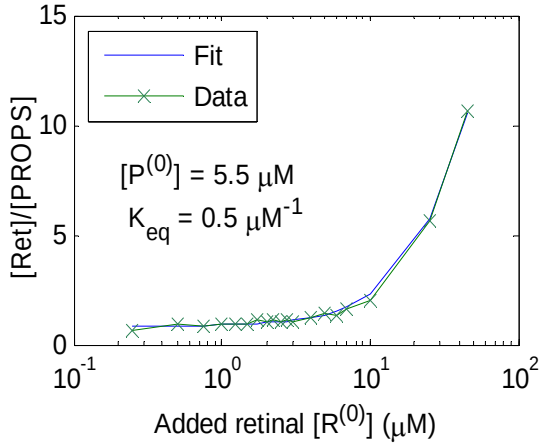

Titration of the quantity of PROPS in an *E. coli* by its ability to bind retinal.

Effect of PROPS expression on cell growth

E. coli strain BW25113 was grown in a 50 mL culture in a shaker at 33 ºC to OD600 of 0.4 (5 hrs.). The cells were then divided into four 50 mL samples which were exposed to different inducer concentrations and 5 μM retinal. The cells were incubated with agitation in the dark for a further five hours. An inducer concentration of 0.0005% arabinose had minimal effect on the growth, so this concentration was chosen for further experiments with strain BW25113. Other strains and plasmids required separate determinations of the maximum inducer concentration at which the cells remained healthy.

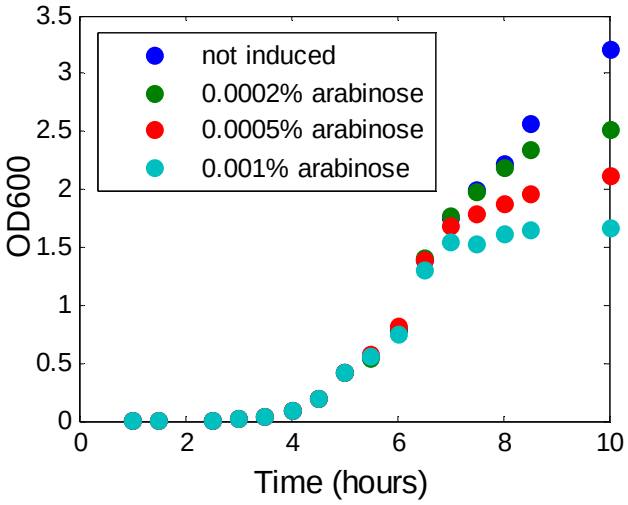

Growth of *E. coli* strain BW25113 as a function of inducer concentration.

Attempts to calibrate voltage response of PROPS

1) Eukaryotic expression

A large number of attempts were made to express PROPS in the plasma membrane of eukaryotic cells, following the protocols of Gradinaru and coworkers *(22)*, as well as other strategies. Efforts included human codon optimization, addition of signaling sequences, golgi and

endoplasmic reticulum export sequences, domain swaps with other microbial rhodopsins having good membrane targeting, variation of protein expression temperature and time, and transfection of multiple cell lines (Supplementary tables S4, S5). All attempts resulted in protein expression localized to the internal membranes of the endoplasmic reticulum (ER), the golgi, or vesicles. No protein was detected in the plasma membrane.

2) Droplet hydrogel bilayers

We attempted to incorporate PROPS into artificial lipid bilayers for the purpose of imaging voltage-dependent fluorescence. Droplet hydrogel bilayers (DHBs) were formed at the interface of a thin agarose pad and a millimeter-scale aqueous droplet immersed in a lipid/oil emulsion. We constructed a custom-machined acrylic sample chamber for the DHB experiments, following Ref. *(23)*. We formed stable DHBs from 1,2-diphytanoyl-sn-glycero-3-phosphocholine (DPhPC), but addition of vesicles comprised of PROPS/DPhPC did not result in PROPS incorporation into the DHB. Addition of small amounts of dodecylmaltoside (0.001-0.005%) to facilitate protein insertion *(24)* resulted in unstable bilayers.

3) Xenopus oocytes

GPR has previously been expressed in xenopus oocytes *(25)*, a model system for electrophysiological studies on membrane proteins. We found that oocytes had intense autofluorescence when illuminated at 633 nm, so we did not attempt protein expression.

4) Patch clamp measurements on E. coli spheroplasts

Delcour and coworkers reported patch clamp studies of *E. coli* spheroplast membranes *(26)*. We formed spheroplasts following literature protocols *(27)*, but found that the patch clamp protocol was incompatible with fluorescence imaging because the membranes were largely sucked into the pipette as soon as suction was applied.

Induced Transmembrane Voltage (ITV)

Cells were immobilized on a poly-(L)-lysine-coated glass coverslip and washed with copious de-ionized water. The coverslip was mounted in an inverted fluorescence microscope. Two steel electrodes (7 mm long, 0.5 mm diameter, separated by 1.6 mm) were mounted on a micromanipulator and positioned on opposite sides of the field of view (Figure below). Voltage pulses from a high voltage amplifier (Trek 2205) were applied to the cells, following the waveform shown below. Pulses alternated polarity to minimize formation of electrochemical byproducts and polarization of the solution. A typical waveform had 1 pulse/s, each pulse lasting 200 ms, and pulse amplitudes ranging from 50 V to 400 V. At the maximum voltage of 400 V, the current was approximately 10 mA. Cells were washed with DI water after every experiment to prevent buildup of electrochemical biproducts.

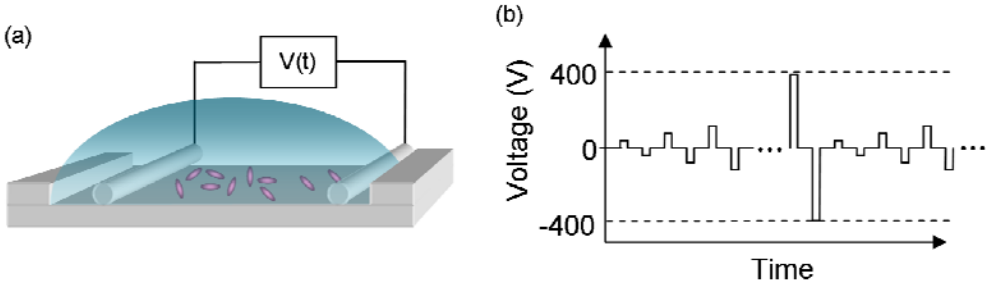

Induced transmembrane voltages applied to *E. coli*. (a) Experimental setup (not to scale). (b) Time-course of voltage pulses. This waveform probed both the fluorescence as a function of voltage, and the dynamic step-response.

In each experiment, a cell whose long axis was parallel to the electric field was selected for analysis. The magnitude of the ITV was proportional to the length of the cell, so usually an elongated cell was selected. To maximize frame rate, we used an Andor iXon^{+} DU-897 camera with a small region of interest (ROI). The camera was externally clocked to synchronize image acquisition with the voltage pulses. Typical exposure times were 0.5 ms. The figure below shows the average changes in fluorescence of a single cell as a function of the ITV.

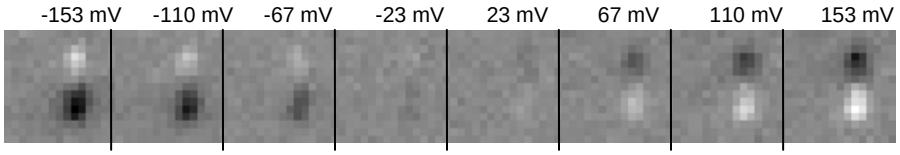

Average deviations in fluorescence as a function of induced membrane voltage in a single *E. coli*. Each image is an average over 10 voltage pulses. λ_{exc} = 633 nm.

We modeled the cell as a conducting prolate spheroid covered with a thin, perfectly insulating membrane. The Schwan equation gives the membrane potential for a spherical cell, and Kotnik and Miklavčič generalized the treatment to include spheroidal cells *(28)*. They showed that the ITV is given by:

$$V(\phi) = E\frac{\left(R_1^2 - R_2^2\right)}{R_1 - \dfrac{R_2^2}{\sqrt{R_1^2 - R_2^2}}\ln\left(\dfrac{R_1 + \sqrt{R_1^2 - R_2^2}}{R_2}\right)} \times \frac{R_2\cos\phi}{\sqrt{R_1^2\sin^2\phi + R_2^2\cos^2\phi}},$$

where E is the electric field strength and the geometrical parameters are defined in the diagram below:

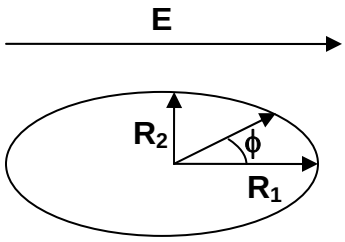

Model of an *E. coli* with its long axis parallel to an electric field.

For a spherical particle ($R_2 = R_1$) the ITV at each pole is $V_{sphere} = \frac{3}{2}ER$. In the limit as the cell becomes long and thin ($R_2/R_1 \rightarrow 0$), the ITV at each pole approaches $V_{line} = ER_1$. We usually picked cells with $R_1 > 5R_2$, in which case the long and thin approximation is adequate.

Calibration of the ITV signal

Direct application of the modified Schwan equation neglects possible voltage drops across the cell wall or outer membrane. To calibrate the ITV procedure we sought a different fluorescent indicator that functioned in *E. coli* and that had a known voltage response. We recently identified a mutant of Archaerhodopsin 3 (Arch) with voltage-indicating properties similar to those of PROPS, but with good membrane targeting in eukaryotic cells. We calibrated the Arch-based sensor by direct patch clamp measurements in HEK cells. Upon expression in *E. coli*, this protein also showed blinking behavior. ITV-induced changes in fluorescence of the Arch-based indicator formed the basis of the calibration.

These measurements indicated that the modified Schwan equation overestimated the voltage drop across the inner membrane by a factor of 3.1, so calculated values were adjusted accordingly. The calibration indicated that under ITV conditions the *E. coli* had a resting membrane potential of $V_0 \sim$ -50 mV. The voltage applied in ITV only induced changes in membrane potential, so the calibration of V_0 was used to position the voltage axis in Fig. 1C. The discrepancy between our measured V_0 and the literature value of -80 to -120 mV is likely due to the fact that ITV experiments were performed on cells that had been sitting for several minutes in deionized water. All other experiments were performed in minimal medium.

Percentage change in fluorescence values ($\Delta F/F$) were calculated as described below in *Image Processing.*

Control experiments in which we imaged fluorescence of Venus in the PROPS-Venus fusion confirmed that the changes in PROPS fluorescence were not due to voltage-induced motion of the entire cell. The Venus fluorescence showed a small ITV signal of opposite sign to the PROPS signal, but at present it is unclear whether this transient was due to changes in local proton activity (Venus shows pH-sensitive fluorescence) or due to changes in nonradiative energy transfer between Venus and the retinal in PROPS.

Calibration of super-ecliptic pHluorin in *E. coli*

Fluorescence excitation spectra were acquired on a bulk solution of pHluorin as a function of pH. The figure below shows the bulk fluorescence under excitation at 488 nm and emission at 509 nm. This excitation wavelength was chosen to match the wavelength used later in microscopic imaging experiments.

PROPS and pHluorin were then co-expressed in *E. coli* strain BW25113. The cells were adhered to a coverslip with poly-L-lysine, and washed with CCCP to equalize pH_i and pH_o. The average fluorescence in the PROPS and pHluorin channels (with simultaneous excitation at 488 and 633 nm) was recorded as a function of pH. The pK_a of pHluorin reported *in vivo* was 7.4 while in bulk it was 7.2. The similarity of the titrations *in vivo* and in bulk confirmed that CCCP set $pH_i = pH_o$. We ascribe the slight difference in pK_a values to imperfect control of the pH in the small sample volumes used in the microscope. This pH error sets the accuracy of single-cell measurements of pH_i to 0.2 pH units. The pH-dependent fluorescence of PROPS showed a broad response, possibly indicative of multiple titratable groups that influenced the fluorescence of the protein.

The precision of single-cell measurements of pH_i was determined by comparing the noise in the pHluorin intensity under nominally constant pH, to the change in pHluorin intensity due to a step from pH 8 to 9. This procedure yielded a shot-noise limited precision of 0.02 pH units/$(Hz)^{1/2}$.

The response speed of pHluorin to pH steps was determined by rapidly exchanging the buffer around CCCP-treated cells. Fig. 2B in the main text shows that this response occurred in < 1 s (limited by the speed of buffer exchange). This result implies that pHluorin responds to changes in local pH faster than 1 s, and that pH changes propagate through the cytoplasm of *E. coli* faster than 1 s. Thus, if blinks in PROPS were accompanied by changes in pH_i of greater than 0.02 pH units, the pHluorin would have indicated these changes.

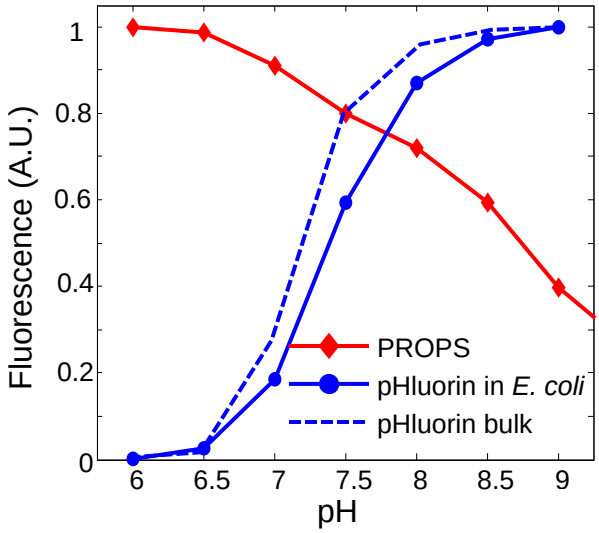

Fluorescence of PROPS and super-ecliptic pHluorin in *E. coli*. Cells were made permeable to protons by treatment with CCCP.

Flagellar rotation assay

A sample of *E. coli* strain JY29 Δ*cheY* was transformed with PROPS and grown as described in Table S2. To shorten the flagella, the cells were sheared approximately 20 times by passage through a 27 gauge needle. Sheared cells were allowed to settle on a clean glass coverslip for several minutes. Some cells attached by a single flagellum and rotated in a circle. Fluorescence movies were acquired which showed simultaneously the rotation and blinking.

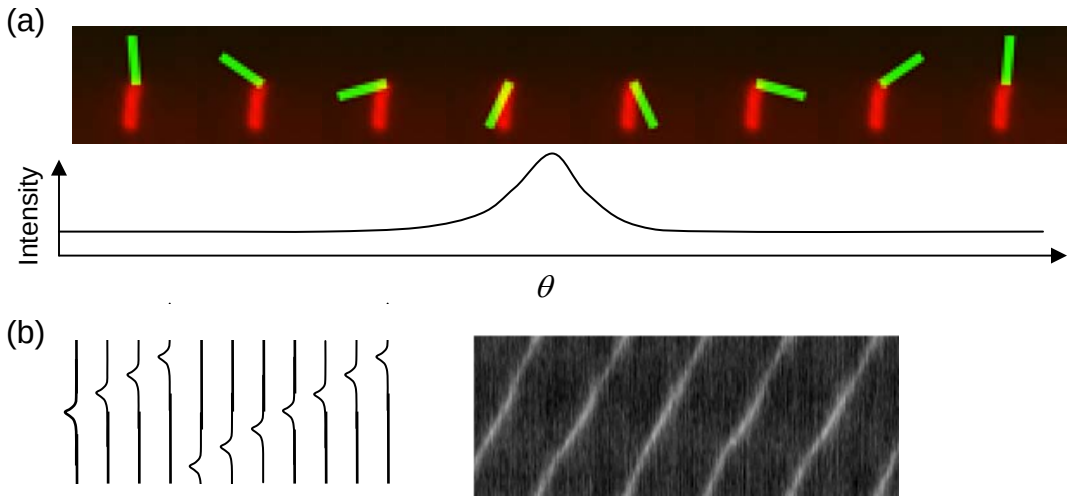

Procedure for constructing a rotary kymogram. (a) For each frame of the movie, the image of the cell (red) is overlapped with a rotating mask (green). The intensity underneath the mask at each rotation angle indicates the angular intensity distribution. (b) Successive intensity distributions are stacked adjacent to each other to create a kymograph which shows intensity of PROPS fluorescence by its brightness, and the angular velocity of the cell by its slope.

Movies were analyzed by constructing "rotary kymographs". For each cell, the center of rotation was identified by examination of an image of time-averaged fluorescence: rotating cells appeared as disks. For each frame, k, we then calculated the angular dependence $I(\theta)$ of the fluorescence brightness within one cell-length of the center of rotation (see figure above). Stacking all of these plots adjacent to each other led to the rotary kymograph, $I(\theta,k)$. Diagonal lines represent rotation at constant angular velocity, with higher slope corresponding to higher angular velocity. The brightness of the diagonal lines indicates the brightness of the cell. In this way it is simple to observe whether blinks coincide with pauses.

Voltage-sensitive dyes

We tested two classes of voltage-sensitive dyes: membrane-localized dyes whose brightness was directly modulated by membrane potential, and Nernstian dyes that accumulated in the cell in a potential-dependent manner. Table S6 lists the dyes that we tested. For Di-4-ANEPPS and Di-8-ANEPPS, cells were pre-incubated with the dye at a concentration between 0.5 and 2 μM in minimal medium, pH 7.5. Cells were then allowed to settle on a coverslip coated with poly-L-lysine, or were immobilized at the interface of an agarose pad and a coverslip. Simultaneous two-color movies of blinking and dye fluorescence were acquired.

The outer membrane of *E. coli* presents a barrier to entry of many small molecules, creating a challenge for loading fluorescent indicators. To increase the permeability of the membrane, we treated the cells with the chelator ethylenediaminetetraacetic acid (EDTA), following the procedure of Lo and coworkers *(29)*. Neither pre-treatment with EDTA, nor flowing dye solution over the cells during imaging, led to an increase in the fraction of cells that took up Di-4-ANEPPS or Di-8-ANEPPS.

To load cells with TMRM, the cells were incubated in 1 mM EDTA at 37 ºC for 1 min. The cells were then washed and immobilized on an agarose pad and sealed in place with a

coverslip. 1 μL of a solution of TMRM (200 μM) was added to a hole in the glass slide on top of the agarose pad. After several seconds the cells became fluorescent under excitation at 532 or 633 nm. Efflux of TMRM during blinks precluded using this dye as an indicator of membrane potential.

Sample chambers and chemical perturbations

E. coli cells were immobilized and imaged using one of three techniques: (1) poly-L-lysine (PLL) coated coverslips, (2) agarose pads, or (3) sticky flagella immobilization.

(1) Immobilization on PLL. A well of approximately 5 x 10 mm area and 0.7 mm depth was formed on a coverslip by using piece of polydimethyl siloxane (PDMS) sheet. Approximately 5 μL of a solution of 0.01% PLL (Sigma P4707) in water was loaded into the well and allowed to evaporate to dryness. Cells suspended in minimal medium were added to the well and allowed to incubate for 2 min. The well was then washed with copious minimal medium to remove non-adhered cells. A glass slide containing holes for fluid inlet and outlet was reversibly sealed to the top of the PDMS sheet to create an enclosed flow cell (see figure below).

(2) Immobilization on an agarose pad. A mold was constructed by affixing a PDMS sheet of thickness 0.7 mm to a glass slide. The PDMS had a cutout of 10 x 10 mm, which was filled with a molten solution of 1.5% agarose in minimal medium. A second microscope slide was placed on top of the mold to form a flat top surface of the agarose. After the agarose gelled, one slide was removed and 0.7 μL of a suspension of *E. coli* was placed on the pad. As soon as the excess liquid had been absorbed by the agarose, a coverslip was placed on the pad to seal the cells at the agarose-coverslip interface. The remaining microscope slide was replaced with a slide with a small hole in the center, to allow addition of TMRM and diffusion of oxygen to the cells.

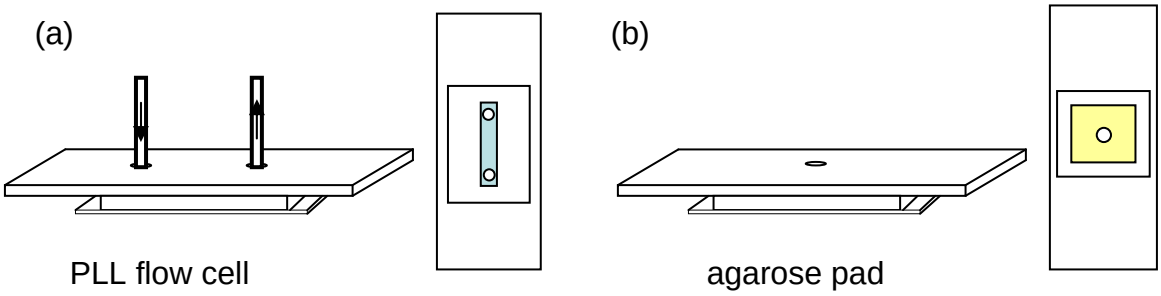

Sample chambers used for imaging. (a) The PLL flow cell allowed rapid exchange of buffer, but some cells retained residual freedom of movement. (b) Immobilization under an agarose pad avoided possible spurious effects from the PLL, but only allowed a single addition of a test chemical through the hole in the top slide.

(3) Immobilization via adhesion of flagella. A suspension of sheared *E. coli* strain JY29 expressing PROPS were was placed in a PDMS well on a clean coverslip and allowed to settle for 10 minutes. The well was then sealed with a glass slide containing inlet and outlet ports. The cells were bathed in a gentle flow of minimal medium, but the flow was stopped during data collection to avoid perturbations to the rotation.

Chemical perturbations were applied by using a syringe pump to change the buffer above the *E. coli*. Flow rates were typically 200 μL/min. We estimate the time for buffer exchange was ~10 s. Unless indicated all buffers were adjusted to maintain constant pH during a perturbation. Oxygen removal was accomplished with Oxyrase (Oxyrase, Inc.) following manufacturer instructions. Oxygen was reintroduced by flowing freshly aerated buffer.

Image processing

All data were analyzed in Matlab (R2009, Mathworks) using custom image processing scripts.

We used covariance-based techniques to automatically identify blinking cells. A simple approach to finding blinkers is to calculate the variance in the fluorescence at each pixel: more variable pixels correspond to blinkers. However, this approach is contaminated by the Poisson-distributed shot noise from bright but non-blinking pixels, which contributes a variance proportional to the intensity. We instead calculated the covariance of the intensity in each pixel with the intensity of its neighboring pixels in space (1 pixel over), and time (1 frame later). The shot noise is uncorrelated between frames and pixels, so this approach is immune to constant background fluorescence. The figure below shows the result of such a calculation, in which the covariance-based measure of blinkiness is displayed in green, and the average brightness is displayed in red. Cells whose covariance intensity exceeded a threshold were deemed to have blinked.

Cells were identified by an automated segmentation algorithm, supplemented by manual scission of closely spaced cells that were marked as one, and manual removal of debris misidentified as a cell. The algorithm could be run either on the covariance image which showed only blinking cells, or on all cells.

Intensity traces were extracted for each cell, with all pixels inside the cell weighted equally. A background intensity trace was calculated from an annulus of pixels surrounding each cell. In cases where cells were immediately adjacent, a partial annulus that did not overlap the adjacent cell was used to calculate background. Fractional changers in fluorescence, $\Delta F/F$, were calculated on the background-subtracted intensity traces, with F taken to represent the baseline (dark state) fluorescence.

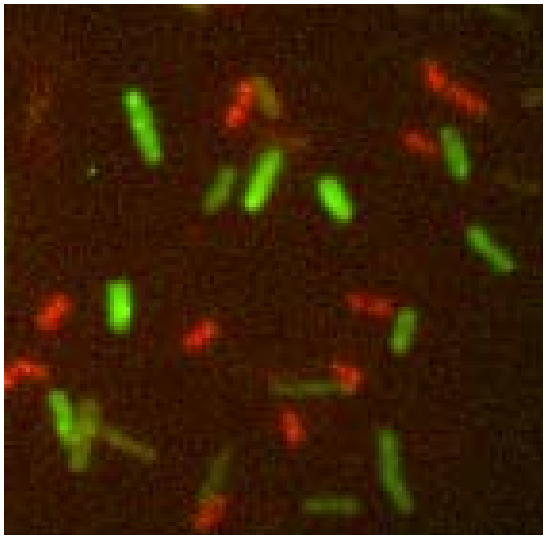

Covariance-based identification of blinking cells. The time-average fluorescence is in red, and the pixel-wise nearest-neighbor covariance is in green. Green cells blinked.

Single-cell intensity traces were analyzed for blink amplitude, duration, and inter-blink interval. This parsing was somewhat subjective because of the wide variety of blink dynamics. The duration of a blink was defined as the full width at half-maximum intensity. Rise times were defined as the time for the intensity to go from 20% to 80% of the maximum for that blink.

To analyze two-color data, images from the two halves of the EMCCD were overlaid. One image was subjected to translation, rotation, and a small change in magnification to maximize its overlap with the other image. Drift during

long movies was removed by registering images to the first frame of the movie. In all cases, transformed images were generated by bicubic interpolation from the original. Images were also corrected for nonuniformities in the illumination spot. Reference images of the illumination spot were acquired for each color, and images were divided by this reference.

Quantifying blinking as a function of laser power

We assayed blinkiness by counting the fraction of cells that blinked at least once during a 200 s observation. The timescale of blinking was determined by fitting the autocorrelation of the fluorescence intensity to a single exponential decay.

Supplementary Text

Design principles underlying PROPS

Here we present a simple model of the voltage sensitivity in PROPS. This model guided our design of PROPS, but it likely neglects many important features of the real protein.

The key idea is that protonation of a titratable group depends on both bulk pH and local electrostatic potential. The local electrostatic potential is partially determined by the membrane potential.

Figure S2 illustrates the physical picture. We assume that the titratable group is primarily coupled to the cytoplasm (based on data described below). The cytoplasm acts as a reservoir of protons at constant chemical potential, given by pH_i. The local electrochemical potential at the titratable group is

$$\mu_{H^+} = V_{loc} + 59\,\mathrm{mV} \times \mathrm{pH_i},$$

where V_{loc} is the local electrostatic potential, measured relative to the cytoplasm, and pH_i is the internal (cytoplasmic) pH. An increase in V_{loc} of 59 mV is equivalent to an increase in pH of 1 unit at room temperature. The titratable group reaches thermal equilibrium by exchanging a proton with the cytoplasm. Thus the pK_a of the titratable group is $\mathrm{pK_a} = \mathrm{pK_a^{(0)}} - \mathrm{V_{loc}}/59\,\mathrm{mV}$, where $\mathrm{pK_a^{(0)}}$ is the pK_a in the absence of a membrane potential.

Most of the voltage drop between the periplasm and the cytoplasm occurs in the double layers on either side of the membrane. These have a thickness given by the Debye length, approximately 0.7 nm. As shown in Figs. S2(B) and (C), V_{loc} is generally smaller in magnitude than V_{m}, though the constant of proportionality is unknown *a priori* (one can think of the protein as a voltage divider with the SB at an intermediate point). Thus one expects a change in membrane potential greater than 59 mV to be equivalent to a change in bulk pH of 1 unit. We measured a correspondence of 102 mV in V_{m} to 1 pH unit, consistent with the above model (Fig. 1C).

Alternatively, deviations from our simple model may contribute to deviations from ideal Nernstian behavior. Membrane potential is likely to affect protonation of many functional groups, some of which will be electrostatically coupled to the SB. These indirect coupling mechanisms could alter the voltage response of PROPS. Additionally, the membrane potential may induce conformational changes in the protein, which could alter the accessibility of the SB, and its local electrostatic potential. If the SB is coupled to both the cytoplasm and the periplasm, then a nonequilibrium Goldman-type treatment is needed to predict the protonation of the SB. Finally, functional groups other than the SB may play a role in determining fluorescence. Membrane potential is likely to regulate the charge state and position of these functional groups as well.

It is important to note that voltage-induced changes in protonation of the SB do not require proton transport across the membrane nor are they accompanied by detectable changes in cytoplasmic pH.

Cytoplasmic accessibility of the SB in PROPS

Our observation that the fluorescence-determining group in PROPS is exposed to the cytoplasm is contrary to the conventional view that the SB in the ground state of microbial rhodopsins is exposed to the extracellular medium *(30)*. Our evidence for the cytoplasm-exposed fluorescence-determining group is:

1) In freshly grown *E.* coli, variation in pH_o causes almost no change in pH_i (reported via pHluorin fluorescence), nor in PROPS fluorescence. After treatment with CCCP, pHluorin fluorescence reports that $pH_o = pH_i$, and PROPS fluorescence becomes sensitive to pH. Thus PROPS fluorescence appears sensitive only to pH_i.
2) ITV experiments and metabolic perturbations both indicate that PROPS fluorescence is bright when the membrane is electrically depolarized, while PROPS is dark in the electrically polarized membrane. This sign of response is consistent with a cytoplasm-exposed titrable group.

There are several possible explanations for this discrepancy between our observations and published structural models.

1) The exposure of the SB in PROPS may be different from in the WT protein. Precedent for this hypothesis comes from molecular dynamics simulations of the bacteriorhodopsin mutant D85N—homologous to D97N in GPR—which found that the mutations switched the accessibility of the SB from the extracellular to the cytoplasmic side.*(31)* Also, experiments on the D75N mutant of sensory rhodopsin II—homologous to D97N in GPR—also showed a transient inward-directed photocurrent, consistent with a cytoplasm-exposed SB (Fig. 4 in Ref. *(32)*).
2) The membrane potential may induce a conformational switch which favors a cytoplasm-exposed SB. Most spectroscopic experiments on microbial rhodopsins are performed without control of the membrane potential, so the conformation in an energized cell may differ from the conformation in a film or in a de-energized vesicle.
3) The voltage sensitivity of PROPS may be determined by a group or groups other than the SB; or by voltage-induced conformational changes in the protein that do not involve shifts in the acid-base equilibrium of the SB.

Additional spectroscopic and computational work is needed to determine the ground-state conformation of GPR D97N (PROPS), and how membrane potential affects this conformation.

Limits on laser heating of *E. coli*

To determine whether heating contributed to the illumination-dependent blinking of *E. coli* we estimate the maximum temperature rise expected under our imaging conditions. The highest intensity used in our experiments was $I = 100$ W/cm^2. We approximate a bacterium as a sphere 2 μm in diameter. If we assume that the cell absorbed *all* of the laser light incident on it, then the power delivered to the cell was $P = 3$ μW. The temperature rise ΔT of a sphere in a homogeneous continuum is given by

$$\Delta T = \frac{P}{4\pi\sigma r},$$

where r is the radius of the sphere and σ is the thermal conductivity of the medium. For our model bacterium in water ($\sigma = 0.58$ W/m K), this estimate yields $\Delta T = 0.4$ °C.

Supplementary Figures

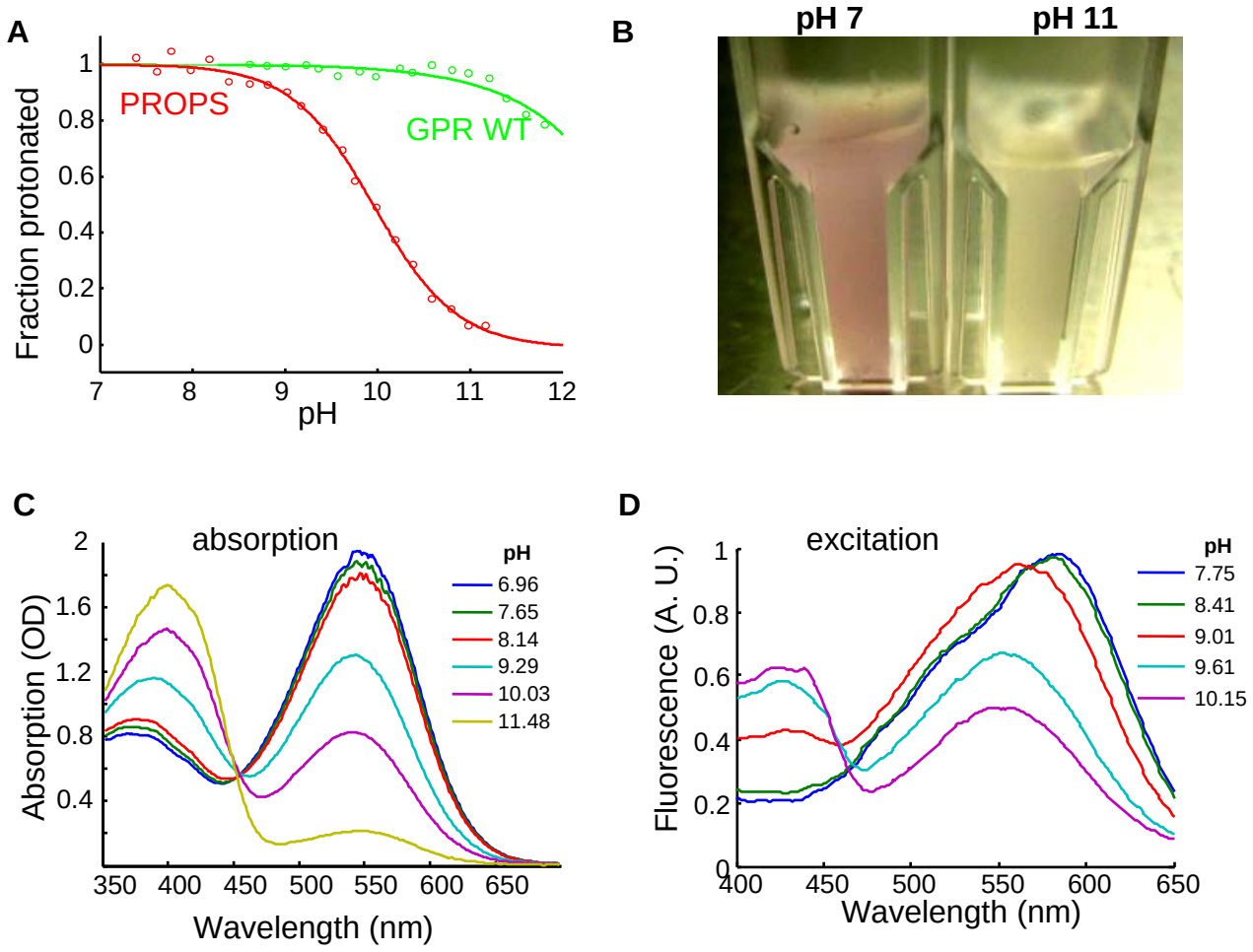

Figure S1. Photophysics of PROPS. (A) Titration of the Schiff Base (SB) in wild-type GPR and PROPS, as measured by visible absorption. We applied Singular Value Decomposition to a series of absorption spectra acquired at different pH values to determine the titration of the Schiff Base (SB). In wild-type GPR, deprotonation of the Schiff Base occurred with a $pK_a > 12$, consistent with earlier reports *(33)*, while in PROPS the pK_a was 9.6. (B) The pH-induced color change in *E. coli* expressing PROPS was visible by eye. (C) pH-dependent absorption and (D) and fluorescence excitation spectra of PROPS. Both quantities showed a pK_a of 9.6, corresponding to protonation of the SB. The apparent shift in the excitation peak between pH 8.41 and 9.01 was an inner filter artifact: to acquire an excitation spectrum in reasonable time, the solution had to be so concentrated that it absorbed a significant portion of the incident light. Test measurements on more dilute solutions showed no shift in excitation spectrum between pH 8 and 9. The data in (C) and (D) imply that protonation of the SB modulated fluorescence by modulating the extinction coefficient at the excitation wavelength

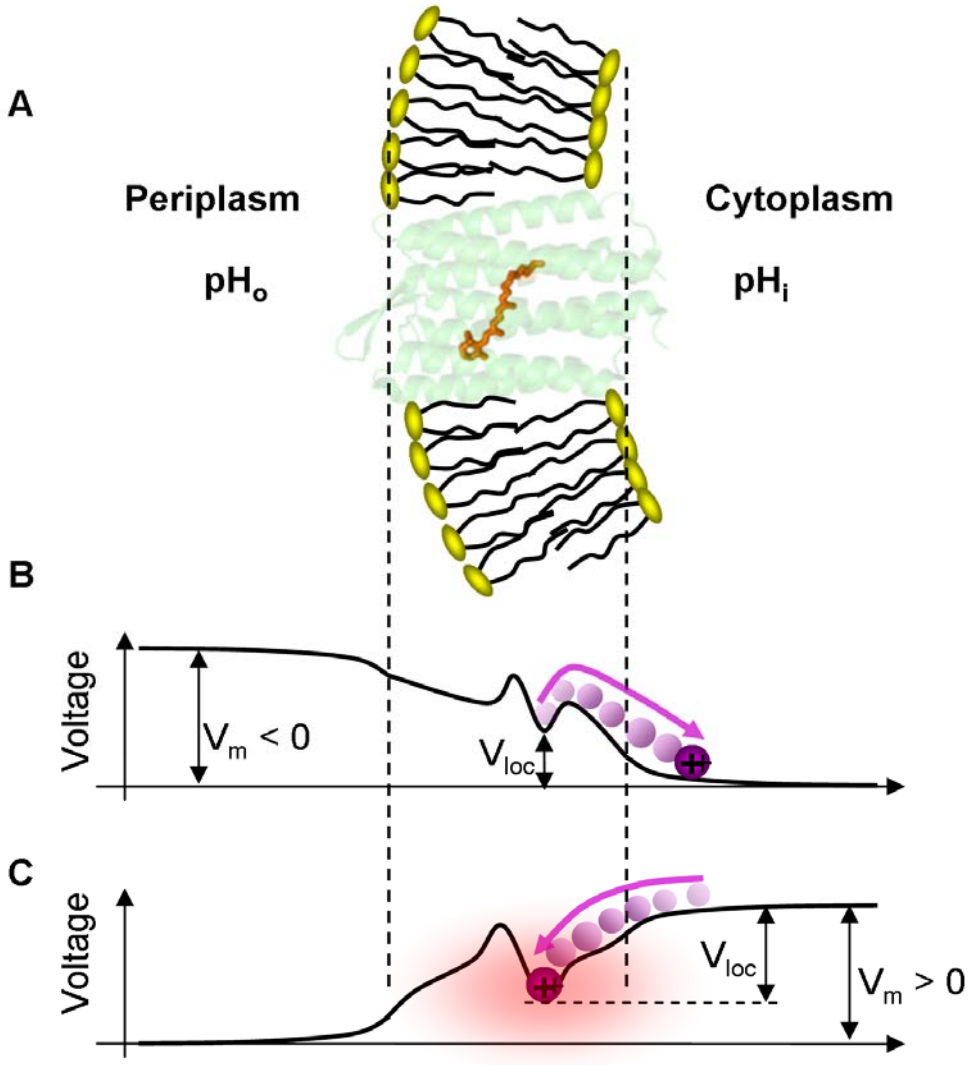

Figure S2. Model of voltage sensitivity in PROPS. (A) Cartoon of PROPS in a lipid bilayer membrane. The structure shown is bacteriorhodopsin; the structures of GPR or PROPS are not known. (B) Potential profile when $V_m < 0$. The potential minimum inside the protein represents the Schiff base (SB). Protons move from the SB to the cytoplasm, causing the protein to become non-fluorescent. (C) Potential profile when $V_m > 0$. Protons move from the cytoplasm onto the SB, causing the protein to become fluorescent. The equilibrium ratio of protonated to deprotonated SB depends on the voltage drop, V_{loc}, between the SB and the cytoplasmic reservoir of protons. The total membrane potential, V_m, is in general greater in magnitude than V_{loc}.

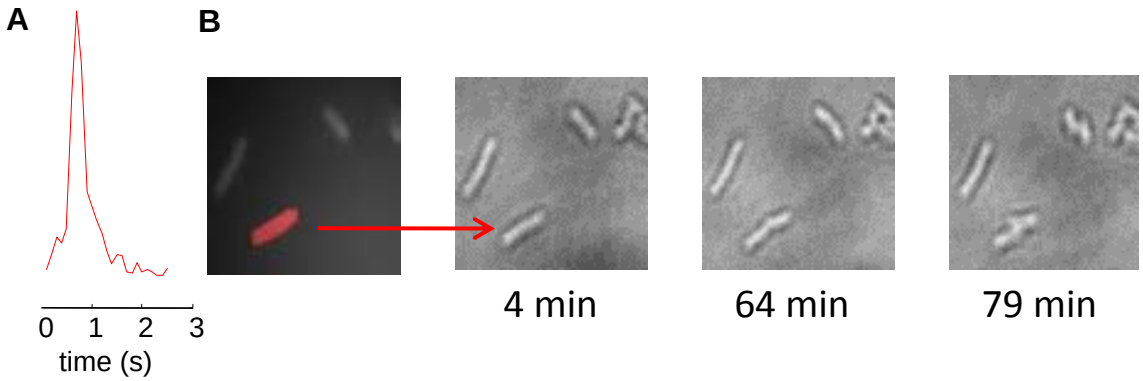

Figure S3. Blinking cells continue to grow and divide. A sample of *E. coli* expressing PROPS was incubated between a glass coverslip and an agarose pad made with minimal medium, pH 7.5. At t = 0 a fluorescence movie was acquired (1 min, 60 W/cm^2), showing blinking cells. The imaging laser was turned off, and the cells were incubated in the dark at 35 ºC. Cells that had initially blinked continued to grow and divide, establishing that blinking cells were alive. (A) Intensity trace showing a single blink from the red-highlighted cell. (B) White-light images showing subsequent growth and division.

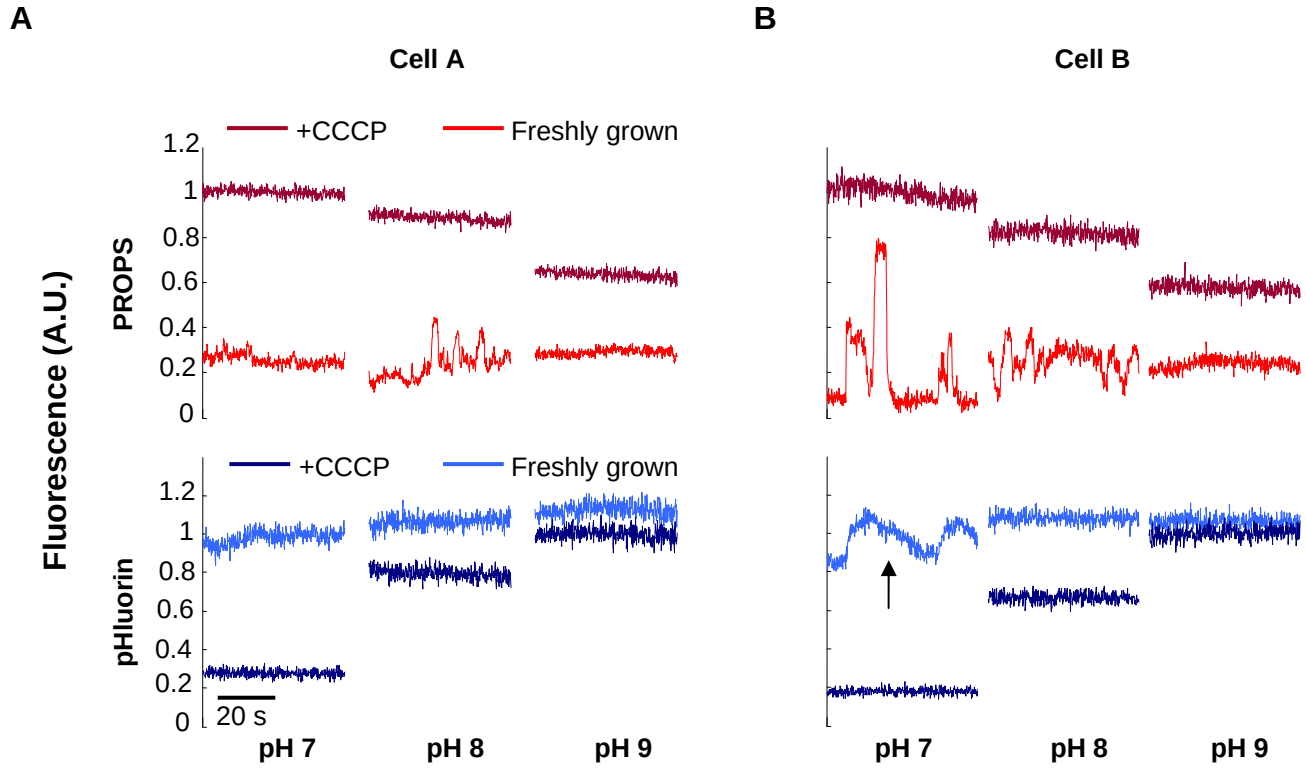

Figure S4. pH_i is constant during spikes in V_m. Fluorescence of PROPS and pHluorin in single *E. coli*, as a function of pH_o, before and after treatment with CCCP. (A) and (B) show data from two representative cells and have the same scale and legend. In freshly grown cells, the fluorescence of pHluorin and PROPS were both only weakly sensitive to pH_o, consistent with

homeostasis of pH_i and a fluorescence-determining group in PROPS not exposed to the extracellular medium. At pH_o = 7, we occasionally observed slow changes in pHluorin fluorescence accompanying large blinks in the PROPS channel (indicated by the arrow in panel b). The timecourse of the changes in pHluorin fluorescence was slower than the changes in PROPS fluorescence and slower than the intrinsic response speed of pHluorin, indicating that variation in pH_i and variation in V_m are distinct processes. At pH_o between 7.5 and 9 we never observed changes in pHluorin fluorescence during a blink.

After treatment with CCCP, pHluorin and PROPS showed pH-dependent fluorescence, confirming a cytoplasm-exposed fluorescence-determining group in PROPS.

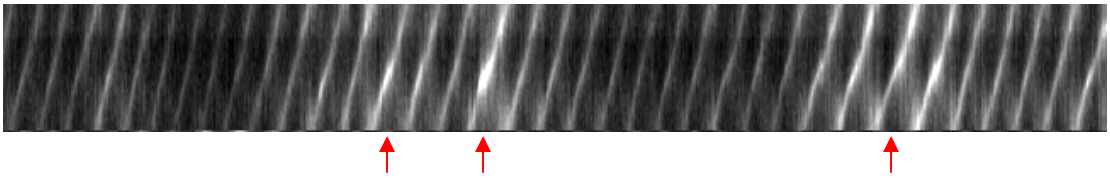

Figure S5. Rotary kymograph at pH_o 7. We only observed a robust correspondence between blinking and loss of flagellar torque at pH_o 8.5. At pH 7, the rotation slowed only slightly during blinks (red arrows). We attribute this pH-dependence to the varying contributions of V_m and ΔpH to the PMF, depending on pH_o. At low pH_o, the PMF was dominated by ΔpH. Only when pH_o was raised so that $pH_o \sim pH_i$ was the PMF determined predominantly by V_m. This condition occurred at $pH_o \sim 8.5$.

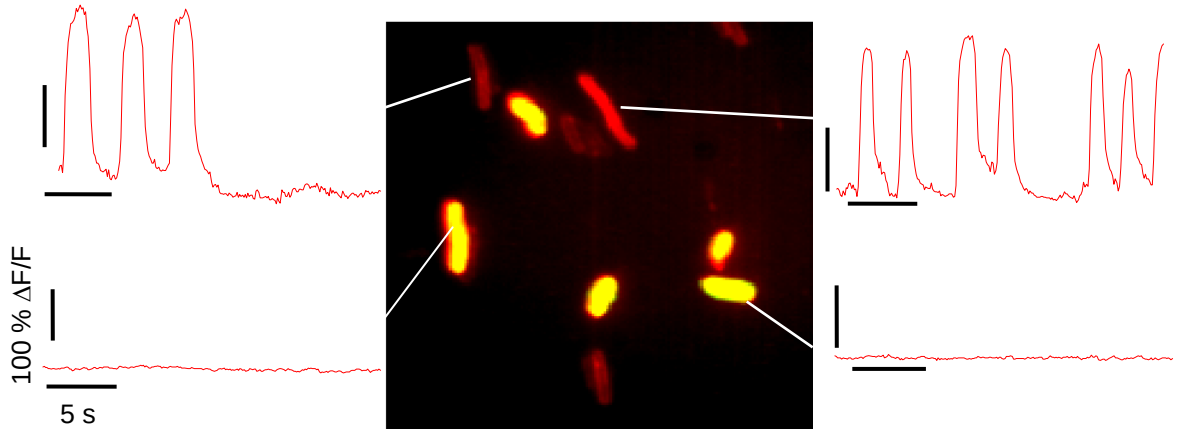

Figure S6. Voltage-sensitive dyes only labeled non-blinking cells. Red channel: PROPS fluorescence; Green channel: Di-4-ANEPPS fluorescence. Cells expressing PROPS and containing dye appear yellow. Red traces indicate PROPS dynamics. All scale bars are 100 % ΔF/F vertical and 5 s horizontal. In every field of view we observed two populations: cells that blinked but that did not take up detectable levels of dye, and cells that took up detectable levels of dye but that did not blink. Washing the cells *in situ* with fresh dye solution did not lead to labeling of blinking cells. Pre-treatment with EDTA also did not lead to labeling of blinking cells. This puzzling observation may be due to blinking-associated efflux, or may be because

blinking requires an intact outer membrane, which is also impermeable to dye. Alternatively, VSDs might inhibit blinking in cells that take up the dye.

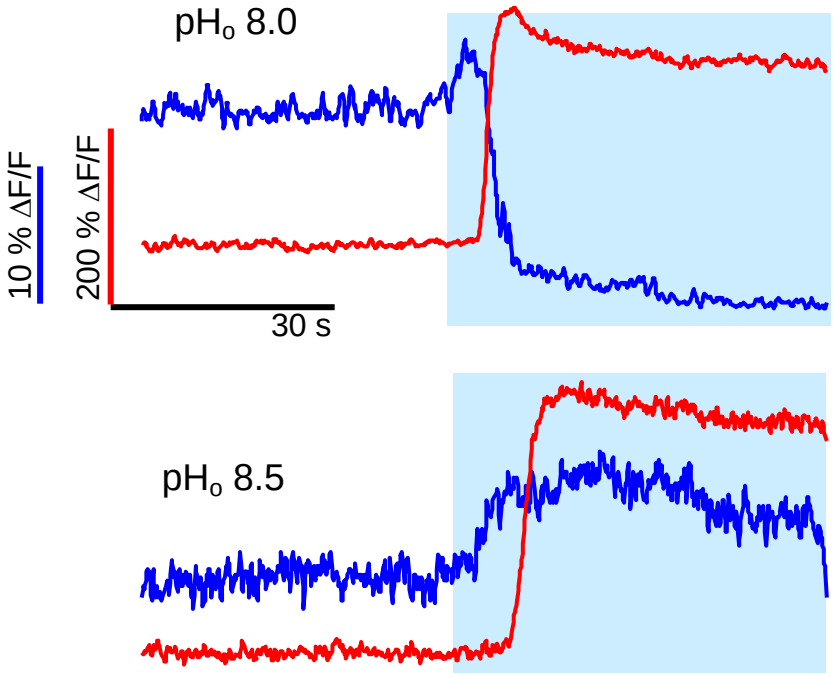

Figure S7. Determination of the value of pH$_o$ at which pH$_i$ = pH$_o$. Cells co-expressing PROPS and pHluorin were equilibrated in buffers with pH$_o$ values between 8 and 8.5 PROPS (red) and pHluorin (blue) fluorescence were monitored during addition of CCCP (50 μg/mL) at constant pH$_o$. Blue bar indicates addition of CCCP. The scale bars are the same for both panels. Addition of CCCP caused pH$_i$ to become equal to pH$_o$, with a corresponding change in pHluorin fluorescence. The case of pH$_i$ = pH$_o$ occurred at pH 8.3, and is shown in Fig. 3D in the main text. At all values of pH$_o$, addition of CCCP caused PROPS to become sharply brighter, indicating electrical depolarization.

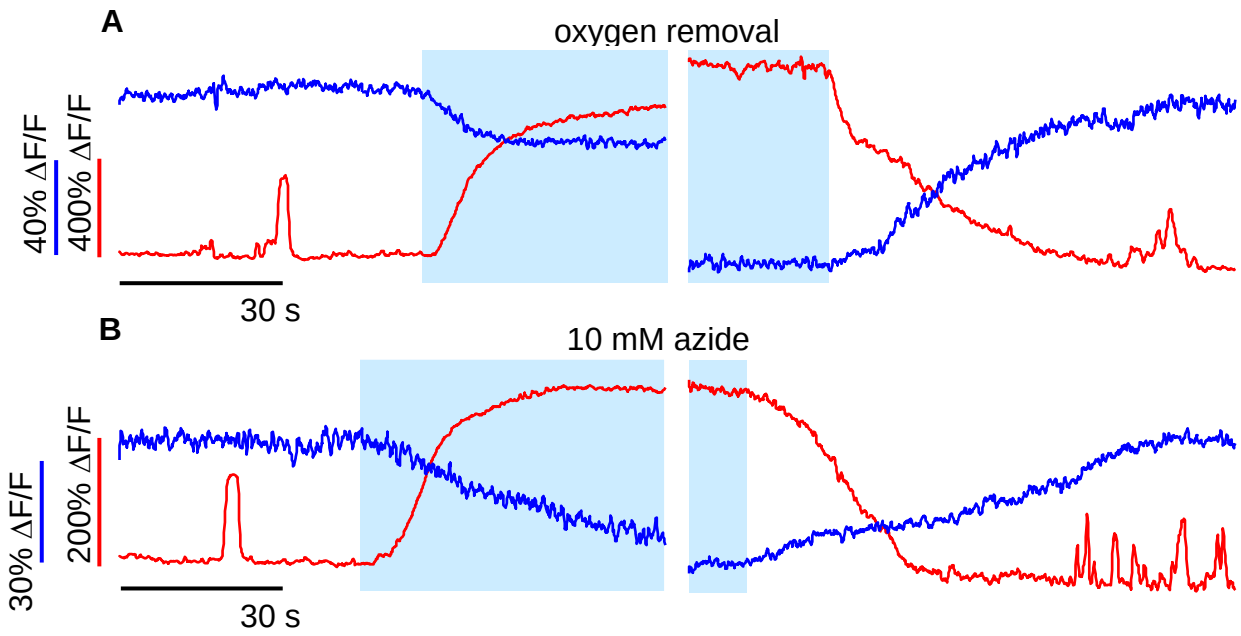

Figure S8. Metabolic perturbations interrupt pH homeostasis. PROPS and pHluorin fluorescence during (A**)** removal and reintroduction of oxygen and (B) addition and removal of sodium azide (10 mM). Data taken with λ_{exc} = 633, 10 W/cm^2 in minimal medium pH 7.5. (B) Removal of oxygen or addition of sodium azide at pH_o 7.5 caused pH_i to gradually equilibrate to pH_o. Reintroduction of regular minimal medium led to restoration of the initial pH_i and resumption of blinking.

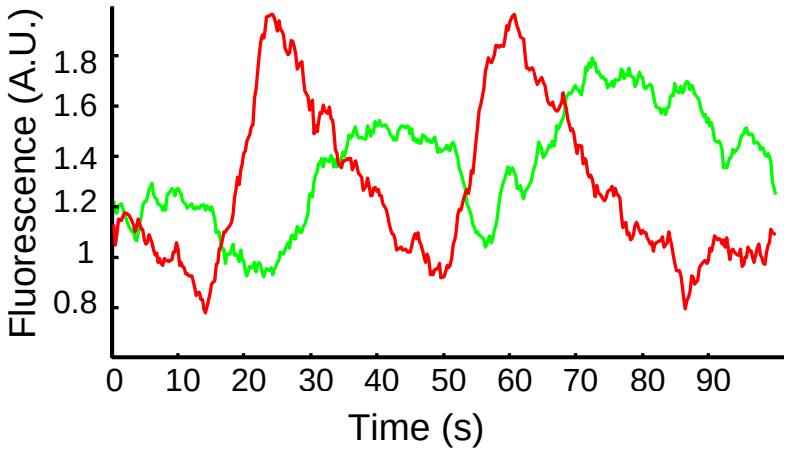

Figure S9. Efflux of TMRM during blinks under dim red illumination (2 W/cm^2 at λ_{exc} = 633 nm, 0.23 W/cm^2 at λ_{exc} = 532 nm), pH 8. We observed efflux of TMRM coincident with blinks of PROPS at the lowest red illumination intensity at which PROPS was observable. In blinking cells containing enough TMRM to record a fluorescent signal, there were noticeable drops in TMRM intensity during a blink, though the TMRM fluorescence often recovered after the blink.

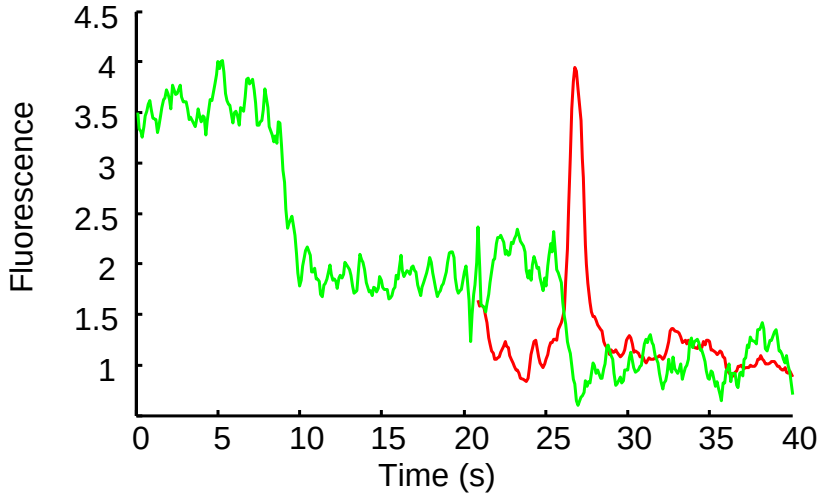

Figure S10. Efflux of TMRM in the absence of red illumination. Fluorescence of a single cell containing PROPS (red) and TMRM (green). The green laser was on for the whole experiment. The red laser was turned on at 20 s at $I = 10$ W/cm^2. Similar efflux events occurred before and after the red laser was turned on; when the red laser was on, efflux was accompanied by a blink in the PROPS channel. These results establish that blinking-associated efflux occurred in the absence of red illumination. Events like that shown here were rare.

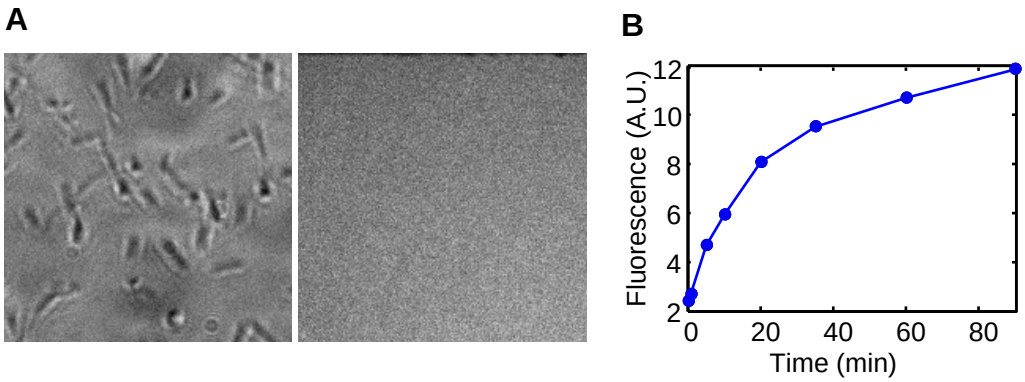

Figure S11. Retinal is necessary for PROPS fluorescence. (A) Left: transmitted light image of a field of cells expressing PROPS but without retinal. Right: fluorescence image of the same field of view. (B) Fluorescence of a single *E. coli* expressing PROPS after 20 μM retinal was added at 0 min.

BL21 (DE3)	*fhuA2 [lon] ompT gal (λ DE3) [dcm] ΔhsdS λ DE3 = λ sBamHIo ΔEcoRI-B int::(lacI::PlacUV5::T7 gene1) i21 Δnin5*
BW25113 (Coli Genome Stock Center)	Δ*(araD-araB)567*, Δ*lacZ4787*(::rrnB-3), lambda-, *rph-1*, Δ*(rhaD-rhaB)568*, *hsdR514*
UT5600	F- *ara-14 leuB6 secA6 lacY1 proC14 tsx-67 Δ(ompT-fepC)266 entA403 trpE38 rfbD1 rpsL109 xyl-5 mtl-1 thi-1*
JY29 (Gift from Howard Berg)	*Thr-1 araC14 leuB6*(Am) *fhuA31 lacY1 tsx-78 λ- eda-50 hisG4(Oc) rfbC1 rpsL136 xylA5 mtl-1 metF159 thi-1* Δ*fliC*, sticky fliC allele was cloned into pACYC184 (CmR) under the native promoter of fliC
Tuner™ (Novagen)	*fhuA2 [lon] ompT gal (λ DE3) [dcm] ΔhsdS λ DE3 = λ sBamHIo ΔEcoRI-B int::(lacI::PlacUV5::T7 gene1) i21 Δnin5 ΔlacZY*

Table S1. Genetic backgrounds of the *E. coli* strains used.

Strain	**Temperature**	**Growth Medium**	**Inducer**	**Antibiotic resistance**
BL21	33 ºC	LB	IPTG 0.5 mM	Amp, Strep (for pHluorin)
BW25113	33 ºC	LB	Ara 0.0005%	Amp
UT5600	33 ºC	LB	Ara 0.02%,	Amp, Strep
JY29	30 ºC	Tryptone broth	IPTG 0.2 mM	Amp, Cm
Tuner™	33 ºC	LB	IPTG 0.5 mM	Amp

Table S2. Growth and induction conditions.

Wavelength	**Power**	**Type**	**Manufacturer**
633 nm	17 mW	HeNe	SpectraPhysics
532 nm	50 mW	Solid-state	Coherent 215-M
488 nm	60 mW	Solid-state	Omicron PhoxX
407 nm	80 mW	Solid-state	Blue-ray DVD player
White light, wavelength selectable via AOTF	6 W	Supercontinuum	Fianium SC-450-6-AOTF
460 – 490 nm	3 W	Luxeon III	Philips

Table S3. Light sources used in the experiments. Multiple wavelengths were combined with appropriate dichroic mirrors.

Plasmid	**Gene**	**Targeting to eukaryotic plasma membrane**
pADD161	ss(A) – GPR	No
pADD173	ss(A) – hGPR	No
pADD191	ss(A) – hGPR – Venus	No
pADD192	ss(B) – hGPR – Venus	No
pADD193	ss(B) – hGPR – Venus – ER export	No
pADD194	ss(C) – hGPR – Venus	No

pADD195	ss(C) – hGPR – Venus – ER export	No
pADD206	ss(A) – hGPR – TS – Venus – ER export	No
pADD210	ss(B) – hGPR – TS – Venus – ER export	No
pADD211	ss(C) – hGPR – TS – Venus – ER export	No
pADD221	ss(A) – hGPR – TS – ER export	No
pADD223	ss(A) – hGPR – TS – G export – ER export	No
pADD224	ss(A) – hGPR – TS – Venus – G export – ER export	No
pADD226	XC(HR) – hGPR – TS – Venus – ER export	No
pADD227	XC(BR) – hGPR – TS – Venus – ER export	No
pADD222	SS(C) – Venus – hGPR – TS – ER export	No
pADD228	SS(C) – Venus – hGPR – TS – G Export – ER export	No

Table S4. Gene constructs tested in attempt at eukaryotic expression of PROPS. **GPR** – bacterial codon GPR, **hGPR** – human codon GPR, **ss(A)** – endogenous GPR signal sequence, **ss(B) -** B2 nicotinic acetylcholine receptor signal sequence, **ss(C)** – bovine pre-prolactin signal sequence, **ER export** – KIR ER export motif; FCYENEV, **TS –** Kir trafficking sequence, **G export** – Kir golgi export motif, **XC(BR)** – extracellular domain from bacteriorhodopsin, **XC(HR)** – extracellular domain from halorhodopsin.

Cell Line	**Plasmid**	**Temperature**	**Targeting to eukaryotic plasma membrane**
HEK 293	All plasmids	30 and 37 °C	No
3T3	pADD223, pADD227	30 and 37 °C	No
HeLa	pADD223,pADD227	30 and 37 °C	No
COS7	pADD223,pADD227	30 and 37 °C	No

Table S5. Cell lines tested for eukaryotic expression.

Voltage Sensitive Dye	**Excitation wavelength (nm)**	**Labeled blinking cells**
Di – 4 – ANEPPS	488	No
Di – 8 – ANEPPS	488	No
TMRM	532	Yes, but effluxed during blinks

Table S6. Voltage sensitive dyes attempted in *E. coli*.

Supplementary Movie 1. *E. coli* strain BW25113 expressing PROPS imaged under high red light intensity (λ = 633 nm, I = 20 W/cm^2). Cells were in minimal medium (pH 8) at room temperature. Movie is sped up by 4x.

Supplementary Movie 2. *E. coli* strain BW25113 expressing PROPS imaged under low red light intensity (λ = 633 nm, I = 1 W/cm^2). Cells were in minimal medium (pH 7) at room temperature. Movie is sped up by 8x.

Supplementary Movie 3. *E. coli* strain JY29 expressing PROPS adhered to a coverslip by a sticky flagellum. Cells were in minimal medium (pH 8.5). Movie is slowed down by 3x.

Supplementary Movie 4. *E. coli* strain BW25113 expressing PROPS exposed to violet light (λ = 407 nm, I = 100 W/cm^2) while imaging PROPS (λ = 633 nm, I = 20 W/cm^2). Cells were in minimal medium (pH 7) at room temperature. Movie is sped up by 6x.

Supplementary Movie 5. *E. coli* strain BW25113 expressing PROPS during oxygen removal with the chemical system Oxyrase. Oxyrase was dissolved in minimal medium (pH 7) according to the manufacturer's directions. Imaging at λ = 633 nm, I = 20 W/cm^2. Movie is sped up by 6x.

Supplementary Movie 6. *E. coli* strain BW25113 expressing PROPS during azide addition (10 mM). Imaging at λ = 633 nm, I = 20 W/cm^2. Movie is sped up by 6x.

Supplementary Movie 7. *E. coli* strain BW25113 expressing PROPS during CCCP addition (50 μg/mL). Imaging at λ = 633 nm, I = 20 W/cm^2. Movie is sped up by 6x.

References and Notes

1. B. Martinac, Y. Saimi, C. Kung, Ion channels in microbes. *Physiol. Rev.* **88**, 1449 (2008).

2. O. Béjà, E. N. Spudich, J. L. Spudich, M. Leclerc, E. F. DeLong, Proteorhodopsin phototrophy in the ocean. *Nature* **411**, 786 (2001).

3. O. Béjà *et al*., Bacterial rhodopsin: Evidence for a new type of phototrophy in the sea. *Science* **289**, 1902 (2000).

4. J. L. Spudich, C. S. Yang, K. H. Jung, E. N. Spudich, Retinylidene proteins: Structures and functions from archaea to humans. *Annu. Rev. Cell Dev. Biol.* **16**, 365 (2000).

5. P. Kolodner, E. P. Lukashev, Y. C. Ching, D. L. Rousseau, Electric-field-induced Schiff-base deprotonation in D85N mutant bacteriorhodopsin. *Proc. Natl. Acad. Sci. U.S.A.* **93**, 11618 (1996).

6. Materials and methods are available as supporting material on *Science* Online.

7. A. K. Dioumaev, J. M. Wang, Z. Bálint, G. Váró, J. K. Lanyi, Proton transport by proteorhodopsin requires that the retinal Schiff base counterion Asp-97 be anionic. *Biochemistry* **42**, 6582 (2003).

8. G. Pucihar, T. Kotnik, D. Miklavčič, Measuring the induced membrane voltage with Di-8-ANEPPS. *J. Vis. Exp.* **33**, 1659 (2009).

9. G. Miesenböck, D. A. De Angelis, J. E. Rothman, Visualizing secretion and synaptic transmission with pH-sensitive green fluorescent proteins. *Nature* **394**, 192 (1998).

10. D. C. Fung, H. C. Berg, Powering the flagellar motor of *Escherichia coli* with an external voltage source. *Nature* **375**, 809 (1995).

11. D. Novo, N. G. Perlmutter, R. H. Hunt, H. M. Shapiro, Accurate flow cytometric membrane potential measurement in bacteria using diethyloxacarbocyanine and a ratiometric technique. *Cytometry* **35**, 55 (1999).

12. G. D. Sprott, W. G. Martin, H. Schneider, Differential effects of near-UV and visible light on active transport and other membrane processes in *Escherichia coli*. *Photochem. Photobiol.* **24**, 21 (1976).

13. T. Noumi, M. Maeda, M. Futai, Mode of inhibition of sodium azide on H^+-ATPase of *Escherichia coli*. *FEBS Lett.* **213**, 381 (1987).

14. A. K. Joshi, S. Ahmed, G. Ferro-Luzzi Ames, Energy coupling in bacterial periplasmic transport systems. Studies in intact *Escherichia coli* cells. *J. Biol. Chem.* **264**, 2126 (1989).

15. W. J. Ingledew, R. K. Poole, The respiratory chains of *Escherichia coli*. *Microbiol. Rev.* **48**, 222 (1984).

16. C. J. Lo, M. C. Leake, T. Pilizota, R. M. Berry, Nonequivalence of membrane voltage and ion-gradient as driving forces for the bacterial flagellar motor at low load. *Biophys. J.* **93**, 294 (2007).

17. J. A. Bohnert, B. Karamian, H. Nikaido, Optimized Nile Red efflux assay of AcrAB-TolC multidrug efflux system shows competition between substrates. *Antimicrob. Agents Chemother.* **54**, 3770 (2010).

18. T. Nagai *et al*., A variant of yellow fluorescent protein with fast and efficient maturation for cell-biological applications. *Nat. Biotechnol.* **20**, 87 (2002).

19. V. Bergo, E. N. Spudich, J. L. Spudich, K. J. Rothschild, Conformational changes detected in a sensory rhodopsin II-transducer complex. *J. Biol. Chem.* **278**, 36556 (2003).

20. N. Ruiz, S. S. Chng, A. Hiniker, D. Kahne, T. J. Silhavy, Nonconsecutive disulfide bond formation in an essential integral outer membrane protein. *Proc. Natl. Acad. Sci. U.S.A.* **107**, 12245 (2010).

21. R. I. Shrager, Chemical transitions measured by spectra and resolved using singular value decomposition. *Chemom. Intell. Lab. Syst.* **1**, 59 (1986).

22. V. Gradinaru *et al*., Molecular and cellular approaches for diversifying and extending optogenetics. *Cell* **141**, 154 (2010).

23. A. J. Heron, J. R. Thompson, B. Cronin, H. Bayley, M. I. Wallace, Simultaneous measurement of ionic current and fluorescence from single protein pores. *J. Am. Chem. Soc.* **131**, 1652 (2009).

24. M. A. Holden, D. Needham, H. Bayley, Functional bionetworks from nanoliter water droplets. *J. Am. Chem. Soc.* **129**, 8650 (2007).

25. T. Friedrich *et al*., Proteorhodopsin is a light-driven proton pump with variable vectoriality. *J. Mol. Biol.* **321**, 821 (2002).

26. A. H. Delcour, B. Martinac, J. Adler, C. Kung, Modified reconstitution method used in patch-clamp studies of *Escherichia coli* ion channels. *Biophys. J.* **56**, 631 (1989).

27. B. Martinac, M. Buechner, A. H. Delcour, J. Adler, C. Kung, Pressure-sensitive ion channel in *Escherichia coli*. *Proc. Natl. Acad. Sci. U.S.A.* **84**, 2297 (1987).

28. T. Kotnik, D. Miklavcic, Analytical description of transmembrane voltage induced by electric fields on spheroidal cells. *Biophys. J.* **79**, 670 (2000).

29. C. J. Lo, M. C. Leake, R. M. Berry, Fluorescence measurement of intracellular sodium concentration in single *Escherichia coli* cells. *Biophys. J.* **90**, 357 (2006).

30. U. Haupts, J. Tittor, E. Bamberg, D. Oesterhelt, General concept for ion translocation by halobacterial retinal proteins: the isomerization/switch/transfer (IST) model. *Biochemistry* **36**, 2 (1997).

31. W. Humphrey, E. Bamberg, K. Schulten, Photoproducts of bacteriorhodopsin mutants: a molecular dynamics study. *Biophys. J.* **72**, 1347 (1997).

32. G. Schmies *et al*., Sensory rhodopsin II from the haloalkaliphilic natronobacterium pharaonis: Light-activated proton transfer reactions. *Biophys. J.* **78**, 967 (2000).

33. E. S. Imasheva *et al*., Formation of a long-lived photoproduct with a deprotonated Schiff base in proteorhodopsin, and its enhancement by mutation of Asp227. *Biochemistry* **44**, 10828 (2005).